Experimental Study of Combined steel and BFRP Reinforced Concrete One-Way Slabs

Researcher name: Avin Hasib Abdullah

PhD in Civil Engineering/ Structural Engineering

Abstract

Fiber reinforced polymer (FRP) bars have been used as the main flexural reinforcement in concrete structures in recent decades. It is regarded as a practical alternative building material instead of steel bars. However, the brittleness nature and the high cost of FRP materials are significant challenges that must be addressed. Recently, researchers added steel bars to FRP-reinforced concrete (FRP-RC) beams to improve their flexural ductility while preserving the high strength of FRP bars on the other hand. In this paper, the efficiency of this new combined reinforced technique in one-way concrete slabs is investigated experimentally and theoretically. 15 one-way concrete slabs reinforced with different combination ratios of steel and basalt fiber reinforced polymer (BFRP) bars were tested including four slabs reinforced with only steel or only BFRP bars. Amount of reinforcement, combination ratio of steel to BFRP were the key parameters. The test results revealed that slabs reinforced with combined steel and BFRP bars had a more ductile behavior than BFRP RC slabs. Theoretical analysis predicted ultimate flexural capacity and modes of failure successfully. Two terms were determined: effective reinforcement ratio and critical reinforcement ratio, which can be effectively used in design of concrete members reinforced with combined steel-FRP bars. Also, it was observed that the use of higher degree of over-reinforcement improved the ductility of combined reinforced slabs.

Keywords: FRP RC beam, Flexural ductility, hybrid FRP reinforcement

Introduction

The topic of fiber reinforced polymer (FRP) composite materials has seen a dramatic surge in research attention over the last few decades. They are regarded as a promising candidate in reinforcing structural concrete elements due to advanced qualities such as high tensile strength, durability, corrosion resistance, and lightweight. It is electromagnetically non-conductive therefore it can be successively used in special applications. A study by Benmokrane and Mohamed [1] showed that the use of FRP either in strengthening or as a reinforcing material leads to improve durability of the concrete structures and reducing overall cost of frequently maintenance works. However, it has been reported in the literature that FRP is several times more expensive than traditional steel bars, although its cost is steadily decreased over the past years .FRP materials have a linear stress-strain relationship up to failure and no warning may be noticed before failure when it is used as main reinforcement in RC beams or slabs. Nevertheless, because FRP bars have a low modulus of elasticity, it reduces the flexural stiffness of reinforced concrete members resulting in severe deformation under serviceability conditions. Flexural behavior and strength of concrete beams reinforced with different types of FRP bars was studied experimentally and theoretically in the literature [2-11].

The non-ductile behavior of FRP RC members is a matter of concern that should not be overlooked because it affects safety of human life. ACI 440. 1R-15[12] recommended using FRP reinforcement ratio of ($\rho_f \geq 1.4\rho_{fb}$) (over-reinforced approach) to guarantee a compression failure mode before rupture of FRP bars. Some researchers explored new composite bars consisting of FRP fibers or sheets either bonded or wrapped to a steel core manually or factory fabricated, which have been used as main reinforcement in concrete beams [13-19] or in one-way concrete slabs [20]. Another technology, combining steel and FRP bars as principal longitudinal reinforcement inside concrete beams, has recently been recommended in the literature [21-25]. Comparatively speaking, the combined reinforced technique required less effort and ensured mechanical qualities of reinforcing bars. Besides, steel bars are a ductile strong material that passes through several states during loading process from elastic to yielding and then towards plastic state thus it gives enough warning before failure of the reinforced concrete elements [26]. As a result, adding steel bars to FRP RC beams is seen as a practical and cost-effective way to improve ductility and prevent structural parts from collapsing. It has not, however, been used in one-way concrete slabs.

As a result, this paper examines the flexural strength and behavior of 15 one-way concrete slabs reinforced with different reinforcement ratio of steel, or basalt fiber reinforced polymer (BFRP) or combination of steel and BFRP bars. A design model for calculation of flexural strength of combined steel-BFRP reinforced concrete (RC) one-way slabs will be proposed. Analysis of failure modes will be performed and compared with experimental results. Deformability will be evaluated theoretically and experimentally to study ductility of combined reinforced slabs.

Experimental Work

Slabs Details

The performance of 15 reinforced concrete one-way slabs were investigated, two slabs reinforced with steel bars, two reinforced with BFRP bars and 11 slabs reinforced with different combination ratio of steel and BFRP bars. All the slabs had a load span of 1200 mm and a cross section of 400x80mm width and thickness. The slabs were designed based on the standard of [12] and [26]. The reinforcement ratios in steel RC slabs (control slabs) were varied between the minimum and maximum values required to prevent shear failure, as determined by the ACI-318 [26] concrete shear strength equation ($V_c = 0.17\sqrt{f_c'}bd$). Consequently, the reinforcement ratio of combined reinforced slabs based on that in the control slabs. Latter (S) was used for the slabs while (T) and (B) were used for the reinforcement ratio of steel and BFRP bars, respectively. For example, (S20-T0.18/B0.105) refers to the slab number 20 that was reinforced with 0.18 percent steel bars and 0.105 percent BFRP bars. The shear strength of concrete slabs with pure BFRP reinforcement was checked using [12] as well as another two codes CAN/CSA-S806-12 [27] and ISIS Canada [28]. 8mm steel bars and 6mm sand-coated BFRP bars were used for main reinforcement, whereas 6mm steel bars were used for the transverse direction. The BFRP bars were provided by MagmaTech manufacturing company in UK. For other direction 6-mm steel bars was used and spaced at 180 mm along the slab. More details of the tested slabs are shown in Table 1 and Figs. 1 and 2.

Properties of materials

Ordinary Portland cement and crushed aggregate with a maximum size of 10 mm were used to create the concrete mix. The mix design ingredient is shown in Table 2. 12 cylinders of dimensions 150x300mm were cast to determine concrete compressive strength (fc') on the 28th day and the testing days. Compressometer and Extensometer were used to determine stress-strain curve and modulus of elasticity of concrete (E_c), as shown in Fig. 3. The descending part of the curve was modeled using *fib*-model Code 2010 [29]. The average (E_c) for three tested cylinders was (34495MPa). The tensile strength of concrete (f_t) was determined from split test and the average value of three cylinders was (4.23 MPa). The yield strength of the steel bars was determined using ASTM A370 [30], and the idealized stress-strain curve is shown in Fig. 4. In the tensile strength test of BFRP bars, a new arrangement as anchors was used, which is shown in Fig. 5. The elastic stress-strain relationship of BFRP bars was plotted in Fig. 4. Rupture of BFRP during the tensile test is presented in Fig. 6. Table 3 lists mechanical properties of both steel and BFRP bars that were used in this investigation.

Test set-up and Instrumentation

The slabs were simply supported and loaded under four-point loading. Concentrated load was applied from a hydraulic jack on stiff distributor steel beam, which was measured by a load cell (50T), resulting in two-line loads on the slab. The load was applied continuously until final collapse (at deflection =155 mm and load reduced to greater than 50% of maximum load). The schematic test set-up of the slab is shown in Fig. 7 (a), (b) and (c). Strain gauge was mounted to the primary reinforcement (Steel and CFRP bars) and the concrete slabs. Three linear variable differential transducers (LVDT) were used, one to measure mid-span deflection and the other two installed at end of the slabs to measure the end rotations. Experimental data of loads, deflections, and strains were measured at near time intervals using a data acquisition device coupled to computer software. Two cameras were installed for thorough observation of the crack propagation, and another camera was set up on the computer screen. Figure 7 shows one of the slabs before testing.

Theoretical Investigation

Analysis of Ultimate Flexural Strength

The combined steel-BFRP reinforced concrete (RC) slabs was analyzed based on design model shown in Fig. 8 assuming a perfect bond between tensile reinforcement and surrounding concrete. And the nonlinearity stress distribution in compression is substituted with a rectangular stress block. Based on strain compatibility equations and equilibrium of forces considering contribution of both steel and BFRP bars in equilibrium, stress level in BFRP bars (f_f) for each slab can be calculated using equation (1). The corresponding moment capacity and theoretical ultimate load can be computed using equations (2) and (3). The analysis of flexural strength of combined reinforced slabs is rely on assumption of yielding of steel bars followed by crushing of concrete while stress of FRP bar should be checked from equation (1), which should be less or equal to ultimate tensile stress (f_{fu}). In order to verify the proposed model, the theoretical ultimate loads (P_{th}) and experimental loads (P_{exp}) for the combined steel-BFRP RC slabs are compared in Table 4.

$$f_f = \sqrt{\frac{1}{4}\left(\frac{A_s f_y}{A_f} + E_f \varepsilon_{cu}\right)^2 + \left(\frac{0.85 f_c' \beta}{\rho_f} - \frac{A_s f_y}{A_f}\right) E_f \varepsilon_{cu}} - 0.5\left(\frac{A_s f_y}{A_f} + E_f \varepsilon_{cu}\right) \leq f_{fu} \qquad (1)$$

$$M_u = \left(\rho_s f_y + \rho_f f_f\right) b d_{eff}^2 \left(1 - \frac{0.59\left(\rho_s f_y + \rho_f f_f\right)}{f_c'}\right) \quad (2)$$

$$P_{th} = \frac{M_u}{0.2} \quad (3)$$

Calculation of flexural strength of control slabs with steel bars alone or BFRP bars alone was performed using provided equations by ACI 318-19 [26] and ACI 440.1R-15 [12] as in equations (4) and (5), respectively.

$$M_u = \rho_s f_y b d_s^2 \left(1 - \frac{0.59\rho_s f_y}{f_c'}\right) \quad (4)$$

$$M_u = \rho_f f_f b d_f^2 \left(1 - \frac{0.59\rho_f f_f}{f_c'}\right) \quad (5)$$

Analysis of Failure modes of combined steel-BFRP RC slabs

In strength controlling limit state, consideration of failure modes is very important. Because FRP bars have a higher tensile strength and a lower modulus of elasticity than steel bars, the FRP RC members reaches a balanced state (with rupture of FRP + compression failure) much sooner than steel RC sections [12]. Therefore, various modes of failure are expected in combined steel-BFRP reinforced concrete slabs. In addition, combining these two reinforcing bars in one section might be complex in analysis point of view. Therefore, it should be carefully considered to determine best combination ratio of steel and BFRP bars in order to avoid any unfavorable modes of failure throughout the design process of one-way concrete slabs reinforced with combined reinforcement in the future. The arrangement of reinforcement inside the concrete slabs in this paper was at one layer. This arrangement is not expected to reduce or eliminate corrosion problem of steel bars with addition of BFRP bars rather than enhancing flexural strength of steel RC slabs from one hand and improving stiffness and ductility of FRP RC slabs with addition of steel bars from the other hand.

The failure modes of combined reinforced slabs can be analyzed using two reinforcement ratio terms: effective reinforcement ratio and critical reinforcement ratio, which are denoted as ($\rho_{s,com}$) and ($\rho_{f,com}$), respectively. They both are presented in equations (6 and 7) and based on equilibrium of forces, strain compatibility, and stress block hypothesis offered by (ACI). The BFRP reinforcement area was transferred to equivalent steel reinforcement area in equation (6) utilizing ultimate tensile strength of BFRP to yield strength of steel bars ($\frac{f_{fu}}{f_y}$). To evaluate steel yielding and compression failure mode, the effective reinforcement ratio ($\rho_{s,com}$) will be compared to equation (8), which is the balanced reinforcement ratio of steel RC slabs. The critical reinforcement ratio ($\rho_{f,com}$) will be compared to equation (9), which is the balanced reinforcement ratio of FRP bars, in order to predict BFRP rupture mode. The balanced reinforcement ratio of steel RC slabs is the condition where concrete crushing and steel yielding occur simultaneously, whereas the balanced reinforcement ratio of FRP RC slab can be defined as the ratio where compression failure and FRP rupture occur at the same time [12].

$$\rho_{s,com} = \frac{\left[A_s + A_f \frac{f_{fu}}{f_y}\right]}{b d_{eff}} \quad (6)$$

$$\rho_{f,com} = \rho_f + \frac{A_s}{b d_f} \frac{f_y}{f_{fu}} \quad (7)$$

$$\rho_{bs} = 0.85\beta_1 \frac{f_c'}{f_y} \left(\frac{\mathrm{E}_s\, \varepsilon_{cu}}{\mathrm{E}_s \varepsilon_{cu} + f_y}\right) \quad (8)$$

$$\rho_{bf} = 0.85\beta_1 \frac{f_c'}{f_{fu}} \left(\frac{E_f\, \varepsilon_{cu}}{E_f \varepsilon_{cu} + f_{fu}}\right) \quad (9)$$

Thus, failure modes of combined steel-BFRP reinforced concrete slabs can be theoretically predicted as follows:

1. If $\rho_{s,com} \leq \rho_{bs}$ Section is controlled by steel yielding+ concrete crushing (compression failure)
2. If $\rho_{s,com} < \rho_{bs}$ and $\rho_{f,com} < \rho_{bf}$ Section is controlled by steel yielding + Rupture of FRP
3. If $\rho_{s,com} \leq \rho_{bs}$ and $\rho_{f,com} \geq 1.4\rho_{bf}$ Section is controlled by steel yielding + concrete crushing (compression failure) +FRP not ruptured
4. If $\rho_{s,com} > \rho_{bs}$ Section is controlled by concrete crushing (compression failure) only

Fig. 9 was provided for more explanation on aforementioned analysis of failure mechanisms. These predictions will be compared against experimental failure modes.
A_s and A_f are area of steel and FRP reinforcement, f_y, E_s are yielding stress and modulus of steel bars. ε_{cu} is max concrete compressive strain (0.003). f_{fu}, E_f are the ultimate stress and modulus of elasticity of BFRP bars, $\beta = 0.85 - 0.05(\frac{f_c' - 28}{7})$.

Analysis of Moment-Curvature Relationship

For theoretical analysis of moment curvature relationship of combined reinforced slabs, a plane cross sections and perfect bond between concrete and tensile reinforcement were assumed. Considering equilibrium of forces, strain compatibility equations and stress-strain distribution of Concrete, steel and BFRP reinforcement, the moment-curvature relationship could be computed. The analysis involves calculating the total reinforcement area in the slab based on stiffness factor (E_f/E_s) as shown in Eq. (10). And for each assumed value of strain the stresses in each material can be calculated with corresponding neutral axis depth, curvature and moment. Equation (11) is proposed to be used when the assumed value of strain exceeds the yielding strain of steel bars. Curvature can be calculated using equation (12).

$$(A_s + A_f \frac{E_f}{E_f})\varepsilon_s E_s = 0.85 f_c' b(\beta_1 c) \quad (10)$$

$$A_s f_y + A_f \varepsilon_f E_f = 0.85 f_c' b(\beta_1 c) \quad (11)$$

$$\varphi = \frac{\varepsilon_c}{c} \quad (12)$$

Analysis of Flexural Ductility

Discussion of available Ductility Measurements

The concept of flexural ductility is significant in the design of RC structures, especially when reinforced with FRP bars. This is due to the fact that FRP has a linear elastic nature up to failure. As a result, if ductility standards are not met, it cannot be reliably employed as reinforcement in concrete structures. Ductility was defined in the literature as capability of the structure to absorb energy without critical mode of failure. In most cases, it refers to inelastic deformation that occurs prior to ultimate failure. For steel RC structures, ductility is commonly quantified in terms of ductility index (μ_Δ) or curvature ductility (μ_φ), which is the ratio of ultimate deflection or ultimate curvature to deflection or curvature at first yield of steel bars [31]. Both aforementioned ductility concepts can be used to evaluate ductility of combined reinforced slabs. However, they are not suitable to evaluate ductility of slabs with FRP reinforcement only because FRP bars do not have a yield point. A dimensionless

ductility measure, which was defined by [24] equal to ($\frac{\Delta_u}{L}$), was used to evaluate ductility of FRP RC slabs.

Steel reinforcement is generally recognized for providing ductility in reinforced concrete structures because it experiences inelastic deformation before failure, enabling full strain to develop in the concrete. This necessitates the steel bars consuming a fundamental amount of energy as shown in Fig 10. This behavior is not possible in concrete structures reinforced with FRP bars due to the sudden and linear release of energy at failure [31-32]. To determine ductility, [31] suggested using the ratio of total energy (area under the load-deflection curve) to elastic energy. However, many researchers believe that while evaluating the ductility of FRP RC structures, the deformability factor (D.F) should be taken into account [33-34**].** It was defined by Vijay and GangaRao [35] as follows:

$$\text{Deformability Factor (D.F)} = \frac{\text{Area under moment curvature curve at ultimate}}{\text{Area under moment curvature curve at a limiting curvature}} \quad (13)$$

Through experimental research on measuring the energy absorption of glass FRP RC beams, the authors determined the limiting curvature to be (0.005/d). This is based on ACI 318's serviceability requirements for deflection and crack width [26]. Newhook et al.[31] used strain limit of 0.002 as a limiting curvature for FRP RC beams and 0.0012 for steel RC beams.

Proposed Deformability Factor

In this research, the deformability factor proposed by Vijay and GangaRao [35] was used to experimentally and theoretically compare the ductility of BFRP RC slabs with combined reinforced slabs. However, due to the use of BFRP bars, which differ from GFRP bars in terms of energy absorption characteristics, their limiting curvature of (0.005/d) was not applied. It was proposed to use a deflection limit equal to (span/180) for combined steel-BFRP RC slabs and (span/240) for FRP RC slabs. This quantification of limiting curvature relied on the serviceability criteria for deflection as specified by [26] and [12].

Results and Discussion

Load-Deflection Response

The slabs were separated into different groups based on their critical and effective reinforcement ratio, as shown in Table (5). The load-deflection curves of the tested slabs are plotted in Figs. 11 to 13. In addition, Fig. 14 shows the load-axial stiffness of reinforcement for all the slabs. It can be observed that all the tested slabs have an initial linear phase in load-deflection curves and the end of this phase is identified by the first line of concrete cracking. Consequently, the gradient of load-deflection decreased indicating a reduction in slab stiffness. The drop in load-deflection stiffness, on the other hand, differed amongst slabs. The load-deflection curve Steel RC slabs (S2 and S3) was stiffer than that of other slabs, and combined reinforced slabs followed them. This is also visible in the load-axial stiffness of reinforcement plot in Fig. 14. As a result, with the addition of steel reinforcement, the stiffness of BFRP RC slabs improved, and combined steel-BFRP RC slabs showed a stiffer response than BFRP RC slabs. The load-deflection curves of steel RC slabs had a horizontal post yield line plateau at post cracking stage until ultimate loads. On the other hand, the absence of steel reinforcement in BFRP RC slabs (S7) a reduction in load-deflection curve can be seen at each cracking load and nearly a linear line up to failure with sudden concrete slab fall down at rupture of BFRP bars. Over-reinforced BFRP S8 was more ductile than S7. The reduction in load-deflection

curve in the former was less than S8, and the curve gradually decreased at crushing of concrete at ultimate.

The addition of steel bars to BFRP RC slabs improved the behavior of load-deflection of the latter. S20 is more ductile than BFRP RC S7 (with roughly the same under reinforcement ratio of 0.18 percent and 0.21 percent, respectively), and although the reduction in load of S20 was sharp due to BFRP bar rupture, the slab exhibited some residual ductility up to concrete crushing because the steel bar had not yet reached its rupture point. Furthermore, S22, which has a greater A_s/A_f than S21, behaved more ductile than the latter, with a significantly lower load reduction at cracking loads and a stiffer curve at ultimate, as illustrated in Fig. 11. (b.).

Figure 12 shows combined slabs with a higher critical reinforcement ratio ($\rho_{f,com} > 1.4\rho_{bf}$). The load-deflection curve of steel RC S2 was also included so that it could be compared to S23 and S28, which all have a similar $\rho_{s,com}$). S24 and S26 were separated in Fig 12(d.) for more clarification. It was noticed that all the combined reinforced slabs have a higher ultimate load than S8, which failed under compression. And the higher the ratio of A_s/A_f inside combined reinforced slabs the more the compression failure mode delayed and the more load carrying capacity was achieved. Furthermore, it was noticed that in group B only S24, which has $\rho_{f,com} > 1.8\rho_{bf}$ and A_s/A_f=1.13, failed in compression. This suggests that the $(1.4\rho_{bf})$ prescribed term for compression failure mode of FRP RC members is a conservative term for combined reinforced slabs and can be increased. This will be discussed in the section on failure modes. In addition, as shown in Fig. 12(c and d), increasing the ratio of A_s/A_f in combined reinforced slabs increased the stiffness of the load deflection curve at the pre- and post-yielding stages and reduced the substantial loss in load capacity after ultimate. For example, among the combined slabs, S28 has the greatest A_s/A_f =6.76 and reduction in load capacity at ultimate was only 35%. This reduction in S26 and S23, which have A_s/A_f =2.54 and 1.69, respectively, were 44 and 63 percent of ultimate load. Because of the high ratio of A_s/A_f =6.76, the load-deflection curve of S28 resembled S2 more than the curve of S23. The presence of a BFRP bar in S28 increased the ultimate load by 116% more than in S2.

Load-deflection curves of slabs with critical reinforcement ratio ($\rho_{f,com} > 2\rho_{bf}$) were plotted in Fig 13 (e and f). It can be noticed that increasing the ratio of A_s/A_f resulted in stiffer load-deflection curve at pre and post cracking phase. S27, S29 and S30 cracked at higher load than S25. Because all of the slabs were over-reinforced, they all exhibited ductile behavior, especially when the load was gradually reduced. S30, which has the highest reinforcement ratio, had the maximum increase in load capacity. The curve of S30, which has the highest ratio of A_s/A_f equal to 4.23 among groups C and D, was remarkably comparable to that of steel RC S3.

Cracking Behavior

1st cracking loads for all of the slabs were determined during the test and they are shown in Table 4. The 1st cracking loads in over-reinforced combined reinforced slabs increased as ratio of A_s/A_f rose. S25, S27, S29, S30 and control steel S3 had 1st cracking loads as follows: 13.23, 15.97, 16.22, 16.55 and 23.08 KN. With regard to number of cracks, it was observed that as the reinforcement ratio and A_s/A_f in combined RC slabs increased, so did the number of cracks. In S22, for example, more cracks are found than in S21.

Verification of Theoretical Analysis with Experimental Results

Ultimate Loads

Table 4 lists the experimental and theoretical loads (P_{exp} and P_{th}) of all the tested slabs. In comparison among the slabs, which have same type of reinforcement, the flexural strength rose as the effective reinforcement ratio increased, as seen in steel RC S3, BFRP RC S8 and combined steel-BFRP RC S30. (P_{exp})s of combined reinforced slabs were higher than predicted by the theoretical model demonstrating the safety provided by the model, except in S21, where the ratio of P_{th}/P_{exp} was 1.11. This slab had low amount of steel bar of only 0.18%. Effect of combined steel-BFRP reinforcement technique on enhancement of flexural strength and ductility improvement of concrete slabs can be clearly seen when comparing combined reinforced slabs to control slabs with the same reinforcement ratio. S23 and S28 both exhibited larger ultimate experimental and theoretical loads than S2. BFRP slab S7 failed with brittle slab fall down, whereas combined steel-BFRP slabs S20, S21 and S22 failed without slab fall down due to the presence of steel bars that carried the combined reinforced slabs.

Balanced Reinforcement Ratio and Failure modes of Combined Reinforced Slabs

This section focuses on comparison between predicted and experimental failure modes. All of the slabs' experimental failure modes are presented in Table 4. Fig. 15 (a to i) showed these failure modes with cracking loads and their patterns at ultimate for several combined slabs. Table 5 lists the theoretical effective reinforcement ratio ($\rho_{s,com}$), critical reinforcement ratio ($\rho_{f,com}$) and balanced reinforcement ratios (ρ_{bs}) and (ρ_{bf}). To validate the theoretical analysis of modes of failure they were compared to the experimental results as follows:

- All the combined reinforced slabs had $\rho_{s,com} < \rho_{bs}$ and as evidenced by Table 4's experimental results they all failed due to steel yielding.
- S20 and S22 both failed due to steel yielding followed by rupture of BFRP bars in brittle manner with sudden drop in load-deflection curves. This agree with theoretical analysis and they both had $\rho_{f,com} \leq \rho_{bf}$.
- According to theoretical analysis, the combined reinforced slabs have to fail in compression when $\rho_{f,com} \geq 1.4\rho_{bf}$. However, S23, S26 and S28, which had $\rho_{f,com} = 1.44\rho_{bf}$ to $1.7\rho_{bf}$, failed due to steel yielding without compression failure.
- S24, S25, S27 to S30 they all have $\rho_{f,com} > 1.8\rho_{bf}$ and they all failed due to steel yielding+ concrete crushing (compression failure). Inclined shear cracks formed and intersected with flexure cracks, which propagated to under point loads. These cracks acted as flexure-shear cracks, as shown in Fig. 15 (a,d,f). The theoretical analysis predicted well the flexure failure modes of combined reinforced slabs and the shear failure in S25 and S27 categorized as a secondarily failure mode.

In summary, according to comparison of theoretical and experimental results, the combined reinforced slab will exhibit compression failure mode after steel yielding when $\rho_{s,com} < \rho_{bs}$ and $\rho_{f,com} > 1.8\rho_{bf}$.

Flexural Ductility

The ductility of the tested slabs was measured using three different methods. The ductility of combined reinforced slabs and steel RC slabs is compared using the ductility index (μ). This depended on data of deflection from the test. The deformability factor (D.F) was calculated experimentally and

theoretically based on moment-curvature relationship to compare ductility of combined reinforced slabs with BFRP RC slabs. In addition, the dimensionless ultimate deflection term (Δ_u/L) is used to evaluate ductility of all the slabs. Ductility values were presented in Table 6. The ratio of A_s/A_f of combined reinforced slabs was included to investigate its effect on ductility values. For each group, the theoretical moment-curvature relationship were plotted and compared in Fig. 16 (A-D).

It can be noticed that theoretical and experimental (D.F) differed. This is due to the fact that ($D.F_{exp}$) were calculated depending on experimental data of steel, BFRP and concrete strains; and due to the high deformability of BFRP bars, some data of BFRP strain stopped several seconds before ultimate load. Therefore, theoretical deformability factor ($D.F_{th}$) was often larger than ($D.F_{exp}$). D.F of BFRP S7 (with under reinforcement ratio) reached to 24 while in S8 (with over reinforcement ratio) it was 10.72. D.F for all the combined reinforced slabs in group A and B were less than their counterparts in BFRP RC slabs S7 and S8, suggesting the effective role of steel bars when added to BFRP RC slabs in ductility enhancement. This was also noticed in the plots of moment curvature relationship of combined reinforced slabs compared to BFRP RC slabs. $D.F_{th}$ of combined slabs with a reinforcement ratio less or equal to balanced ratio (slabs in group A) varied from 5 to 8.47. While D.F for slabs with greater critical reinforcement ratio($\rho_{f,com} > 1.4\ \rho_{bf}$) ranged between (6.45 to13).

With regard to Ductility index (μ), in combined reinforced slabs with ($\rho_{f,com} = 1.4\ to\ 1.7\rho_{bf}$) the values of (μ) were extremely high ranging from (18 to 23). Then the value of (μ) declined in slabs with higher reinforcement ratio (failed due to steel yielding followed by compression failure) to between (15 to16.33) in group C and (11.2) in S30 in group D. The value of (μ) in the latter was close to ductility index of S3. Overall, slabs with critical reinforcement ratio greater than $1.4\rho_{fb}$, showed higher ductility indexes than slabs with reinforcement ratio less or equal to balanced reinforcement ratio (group A). Furthermore, in slabs in groups B, C, and D, there was a good interaction between steel and BFRP experimental strain data, and stain data in both reinforcing materials were identical at steel bar yielding. In slabs in group A, however, strain in BFRP bars preceded strain in steel bars following the commencement of the first crack, and the steel tried to follow the BFRP strain, yielding at a higher deflection. For instance, because S22 had (Δ_y) of 12.6mm, its ductility index was the lowest, at only 5.30. S20 was more ductile than S7 but its (Δ_u/L) was greater, indicating that it is not a good ductility measurement for slabs with under reinforcement ratio. This was also demonstrated in Lau and Pam's study [24].

Increasing ratio of A_s/A_f was observed to be more effective in enhancing ductility of slabs with $\rho_{f,com} = 1.4\ to\ 1.7\rho_{fb}$ (group B), where ductility index increased, deformability decreased and (Δ_u/L) become very similar to steel slab S2. However, when the ratio of A_s/A_f was greater than 2.54 (such as S28), the value of (Δ_u/L) increased more than BFRP reinforced slab (such as S8). Furthermore, increasing the ratio of A_s/A_f (in group C) above 3.38 resulted in a drop in the ductility index. As a result, increasing the degree of over-reinforcement achieved ductility improvement and the ratio of A_s/A_f in the range of 2.54-3.38 is found to be a best combination ratio, as far as ductility concerned.

Conclusion

Experimental and theoretical investigation of 15 one-way concrete slabs reinforced with different techniques using either steel or BFRP alone or combined steel-BFRP reinforcement were performed. The following conclusions are drawn.

1. Using a combined steel-BFRP reinforcement technique proved flexural strength enhancement more than using steel reinforcement alone.

2. Adding steel reinforcement to BFRP RC slabs enhanced the stiffness of load-deflection and moment-curvature curves and prevented the sudden brittle failure of BFRP RC slabs.
3. It was discovered that by using a high steel reinforcement ratio the ductility of combined reinforced slabs can be enhanced.
4. For tensile testing of BFRP bars, a new arrangement was employed, which is highly recommended because it saves time and effort compared to steel tubes anchors specified in the literature.
5. Theoretical flexural loads predicted by the model were in good agreement with experimental loads.
6. Theoretical analysis of failure modes was verified by experimental results. It was found that the combined reinforced slab will exhibit compression failure mode after steel yielding when $\rho_{s,com} < \rho_{bs}$ and $\rho_{f,com} > 1.8\rho_{bf}$.
7. The effective reinforcement ratio and critical reinforcement ratio were found to be highly beneficial in predicting modes of failure of combined reinforced slabs, and they can be used effectively in the design of combined reinforced slabs with any type of FRP bars to avoid any unfavorable mode of failure.
8. The 1st cracking loads for all the slabs were determined and the experimental results showed that the higher the effective reinforcement ratio, the lower the ratio of P_{cr}/P_{exp}. Also, the higher the amount of BFRP reinforcement in the combined reinforced slab the less the value of P_{cr}, implying that the first crack will emerge sooner.
9. Three quantifiable measurements were used to evaluate ductility of combined reinforced slabs: ductility index, ultimate deflection term and deformability factor.
10. It was proposed to calculate deformability of BFRP and combined reinforced slabs based on a limiting curvature at L/240 and L/180, respectively.
11. Deformability factor of combined steel-BFRP reinforced concrete slabs with a reinforcement ratio less or equal to balanced ratio varied from 5 to 8.47, whereas in BFRP RC S7 it was 24.
12. Deformability of combined reinforced slabs with higher reinforcement ratio($\rho_{f,com} > 1.4\ \rho_{bf}$) ranged between (6.45 to 8.8), while in BFRP S8 was 10.72.
13. Increasing the degree of over-reinforcement achieved ductility improvement in combined reinforced slabs, and the ratio of A_s/A_f in the range of 2.54-3.38 is found to be a best combination ratio that provides sufficient ductility.
14. All of the combined reinforced slabs provided better ductility performance than BFRP reinforced concrete slabs.

Recommendation for future studies

- This study is believed to contribute to the development of the field of concrete structures reinforced by composite (FRP) materials. Adding steel bars to FRP RC structures promises solving the non-ductile behavior and high cost of these structures. However, further research on ductility performance of combined reinforced one-way concrete slabs reinforced with different types of FRPs (other than BFRP bars) is required. In addition, it is of importance to study shear behavior and strength of one-way concrete slabs or beams reinforced with combined steel-FRP bars. In order to ensure flexure failure mode in one-way concrete slabs reinforced with FRP or combined steel-FRP reinforcement, it is recommended to use a high modulus FRP bars and increasing concrete compressive strength. Furthermore, in order for the combined reinforced

approach to be employed efficiently and widely, a manufacturing standard for FRP bars is essential.

References

1. Benmokrane, B.& Mohamed, H. M. Use of fiber-reinforced polymer (FRP) rebars for building durable concrete infrastructure. In: Proceedings of 2nd RN Raikar Memorial International Conference and Bathia-Basheer Iternational Symposium on Advances in Science and Technology of Concrete, December 18-19, Mumbai, India. https://www.researchgate.net/publication/287995961 (2016).
2. Erfan, A.M., Abd Elnaby, R.M. Badr, A.A. & El-sayed, T.A. Flexural behavior of HSC one way slabs reinforced with basalt FRP bars. *Case Studies in Construction Materials* **14**. https://doi.org/10.1016/j.cscm.2021.e00513 (2021).
3. Adam, M.A., Erfan, A.M., Habib, F.A. & El-Sayed, T.A. Structural Behavior of High-Strength Concrete Slabs Reinforced with GFRP Bars. *Polymer* **13**(17), 2997. https://doi.org/10.3390/polym13172997 (2021).
4. Nasif, M.K., Erfan, A.M,, Fadel, O.T. & El-sayed, T.A. Flexural behavior of high strength concrete deep beams reinforced with GFRP bars. *Case Studies in Construction Materials* **15**. https://doi.org/10.1016/j.cscm.2021.e00513(2021).
5. Erfan, A.M., Algash, Y.A. & El-sayed, T.A. Experimental & Analytical Flexural Behavior of Concrete Beams Reinforced with Basalt Fiber Reinforced Polymers Bars. *International Journal of Scientific & Engineering Research* **10** (8), 297-315(2019).
6. Grace, N.F., Soliman, A.K., Abdel-Sayed, G. & Saleh, K.R. Behavior and ductility of simple and continuous FRP reinforced beams. *J. Compos. Constr* **2** (4),186–194. https://doi.org/10.1061/(ASCE)1090-0268(1998)2:4(186) (1998).
7. Theriault, M. & Benmokrane, B. Effects of FRP reinforcement ratio and concrete strength on flexural behavior of concrete beams. *J. Compos. Constr* 2 (1), 7–16. https://doi.org/10.1061/(ASCE)1090- 0268(1998)2:1(7) (1998).
8. Pecce, M., Manfredi, G. & Cosenza, E. Experimental Response and Code Models of GFRP RC Beams in Bending. *Journal of Composites for Construction* **4**(4), 182. DOI: 10.1061/(ASCE)1090-0268(2000)4:4(182) (2000).
9. Al-Salakawy, E., Kassem, C.H. & Benmokrane, B. Flexural behavior of concrete beams reinforced with carbon FRP composite bars. In: Proceedings of the 4th structural specialty conference of the Canadian Society for Civil Engineering, Montreal, Quebec, Canada. https://scholar.google.com/scholar?q=Flexural+behavior+of+concrete+beams+reinforced+with+carbon+FRP+composite+bars&hl=en&as_sdt=0&as_vis=1&oi=scholart(2002).
10. Wang, H. & Belarbi, A. Flexural Behavior of Fiber-Reinforced-Concrete Beams Reinforced with FRP Rebars. *ACI Structural Journal*, 230-251. https://scholar.google.com/scholar?q=Flexural+Behavior+of+Fiber-Reinforced-Concrete+Beams+Reinforced+with+FRP+Rebars&hl=en&as_sdt=0&as_vis=1&oi=scholart(2005).
11. Goldston, M., Remennikov, A. & Sheikh, M. N. Experimental Investigation of the Behaviour of Concrete Beams Reinforced with GFRP Bars under Static and Impact Loading. *Engineering Structures* 113, 220-232. DOI: 10.1016/j.engstruct.2016.01.044(2016).

12. ACI COMMITTEE 440.1R-15. Guide for the design and construction of structural concrete reinforced with fiber-reinforced polymer (FRP) bars. American Concrete Institution, Farmington Hills, MI., USA. (2015).
13. Henneke, M. J. Evaluation of Hybrid Reinforcement Fiber-Reinforced-Plastic Rod with Steel Core..https://scholar.google.com/scholar?q=Evaluation%20of%20Hybrid%20Reinforcement%20Fiber-Reinforced-Plastic%20Rod%20with%20Steel%20Core(1993).
14. Nanni, A., Henneke, M. J. & Okamoto, T. Tensile Properties of Hybrid Rods for Concrete Reinforcement. *Construction and Building Materials* **8** (1), 27-34. https://doi.org/10.1016/0950-0618(94)90005-1(1994).
15. Saikia, B., Thomas, J., Ramaswamy, A. & Nanjunda, K. S. Performance of Hybrid rebars as Longitudinal Reinforcement in Normal Strength Concrete. *Materials and Structures* **38**, 857-864. Doi:10.1617/14229(2005).
16. Wu, G., Wu, Z., M.ASCE, Luo, Y., Sun, Z. & Hu X. Mechanical properties of steel-FRP composite bar under uniaxial and cyclic tensile loading. *Journal of Materials in Civil Engineering* **22**(10), 1056-1066. DOI: 10.1061/(ASCE)MT.1943-5533.0000110(2010).
17. Park, K. T., Kim, H. Y., You, Y. J., Lee, S. Y. & Seo, D. W. Hybrid FRP Reinforcing Bars for Concrete Structures. In: Proceedings of 4th Asia-Pacific Conference on FRP in Structures, 11-13 December, Melbourne, Australia. (2013).
18. Sun, Z., Yang, Y., Yan, W., Wu, G. & He, X. Moment-Curvature Behaviors of Concrete Beams Singly Reinforced by Steel-FRP Composite Bars. *Advances in Civil Engineering* **1**, 1-14. https://doi.org/10.1155/2017/5691278(2017).
19. Ju, M., Lee, S. & Park, C. Response of Glass Fiber Reinforced Polymer (GFRP)-Steel Hybrid Reinforcing Bar in Uniaxial Tension. *International Journal of Concrete Structures and Materials* **11**(4), 677-686. DOI 10.1007/s40069-017-0212-9(2017).
20. Etman, E. E. Innovative Hybrid Reinforcement for Flexural Members. *Journal of Composites for Construction* **15**, 2-8. DOI: 10.1061/(ASCE)CC.1943-5614.0000145(2011).
21. Aeillo, M. A. & Ombres, L. Structural Performances of Concrete Beams with Hybrid (Fiber-Reinforced Polymer-Steel) Reinforcements. *J. Compos Constr* **6**, 133-140. DOI:10.1061/(ASCE)1090-0268(2002)6:2(133) (2002).
22. Leung, H. Y. & Balendran, R. V. Flexural behaviour of concrete beams internally reinforced with GFRP rods and steel rebar. *Structural Survey* **21**(4), 146-157. DOI 10.1108/02630800310507159(2003).
23. Qu, W., Zhang, X. & Huang, H. Flexural behavior of concrete beams reinforced with hybrid (GFRP and Steel) bars. *J. Compos. Constr* **13**: 350-359. DOI: 10.1061/(ASCE)CC.1943-5614.0000035(2009).
24. Lau, D. & Pam, H. J. Experimental study of hybrid FRP reinforced concrete beams. *Engineering Structures* **32**: 3857-3865. Doi:10.1016/j.engstruct.2010.08.028 (2010).
25. Sui, L., Xing, F., Zhu, J., Li, D. & Liu, J. Experimental study on flexural performance of steel and FRP hybrid-reinforced concrete beams. In: Proceedings of 2nd International Symposium on Service Life Design for Infrastructure, October 4-6, Delft, The Netherlands (2010).
26. ACI COMMITTEE 318. Building code requirements for structural concrete, (ACI318M-19). American Concrete Institution, Farmington Hills, MI., USA. (2019).

27. Canadian Standards Association. Design and Construction of Building Components with Fibre Reinforced Polymers, CSA-S806-12. Rexdale, Ontario, Canada. (2012).
28. ISIS Canada Research Network. Reinforcing Concrete Structures with Fiber Reinforced Polymers, ISIS.M03-07. Winnipeg, Manitoba.: The Canadian Network of Centers of Excellence on Intelligent Sensing for Innovative Structures, The University of Manitoba, Winnipeg, Manitoba. file:///C:/Users/Click/Downloads/Design_Manual_FRP_M3.pdf(2007).
29. International Federation for Structural Concrete (*fib*). Model Code 2010. Lausanne, Switzerland. (2010).
30. ASTM: A370. Standard Test Methods and Definitions for Mechanical Testing of Steel Products. ASTM Committee. DOI:10.1520/A0370-11(2011).
31. Naaman, A.E., & Jeong, S. M. Structural ductility of concrete beams prestressed with FRP tendons, in: L. Taerwe (Eds.), Non-metallic (FRP) reinforcement for concretes structures, E & FN Spoon, London, 379–392. (1995).
32. Alsayed, S.H. & Alhozaimy, A.M. Ductility of concrete beams reinforced with FRP bars and steel fibers. *Journal of Composite Materials* **33**(19), 1792-1806. https://doi.org/10.1177/002199839903301902(1999)
33. Newhook, J., Ghali, A. & Tadros, G. Cracking and deformability of concrete flexural sections with fiber reinforced polymer. *Journal of Structural Engineering* **128**(9), 1195-1201. DOI: 10.1061/(ASCE) 0733-9445(2002) 128:9(1195) (2002)
34. Abdelrahman, A.A., Tadros, G. & Rizkalla, S.H. Test Model for the First Canadian Smart Highway Bridge. *ACI Structural Journal* **92**(4), 451-458. https://www.researchgate.net/publication/266075428(1995)
35. Vijay, P.V. & GangaRao, H.V.S. A unified limit state approach using deformability factors in concrete beams reinforced with GFRP bars; In: Proceedings of the 4th conference on Materials Engineering, November 10-14, Washington, D.C., United States. (1996).

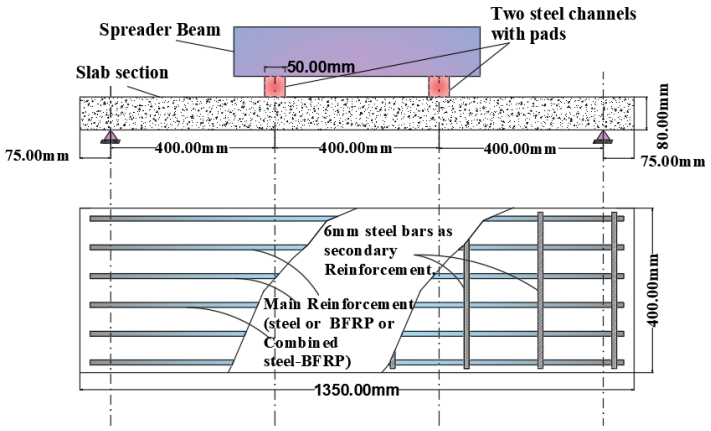

Figure1. Dimensions, details of main and secondary reinforcement and test setup

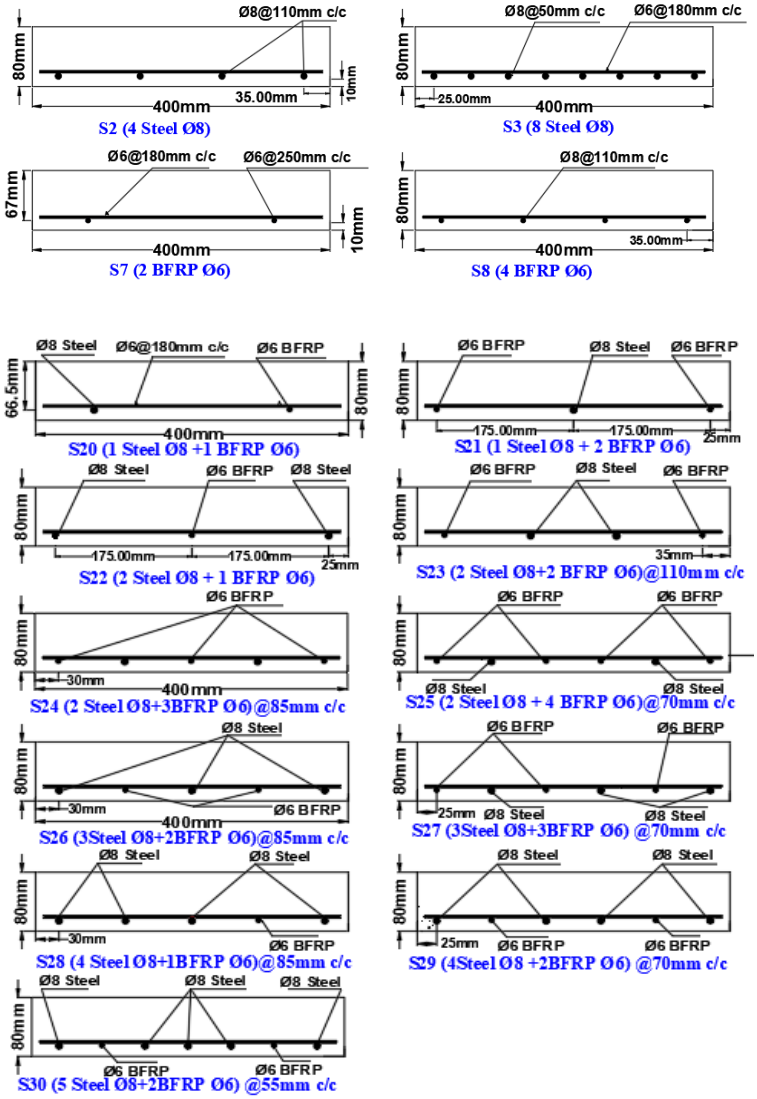

Figure2. Cross-sectional details of all the tested slabs

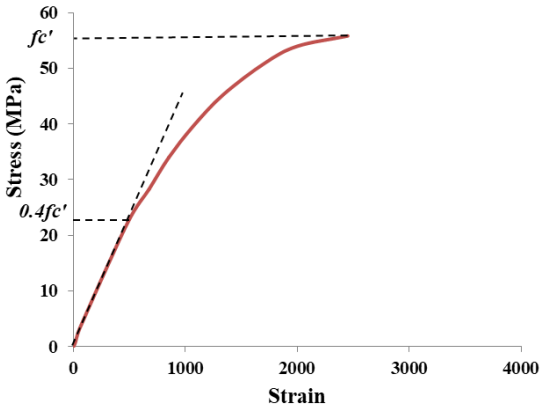

Figure 3. Stress-strain curve of concrete in compression

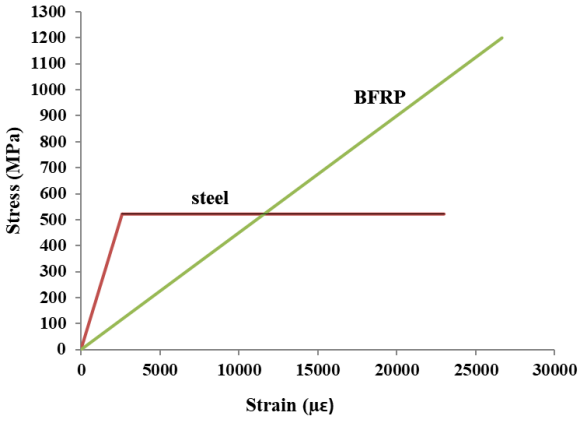

Figure 4. Stress-strain curve of steel and BFRP

Figure 5. Aluminum anchors

Figure 6. Tensile test of BFRP bar with aluminum anchor

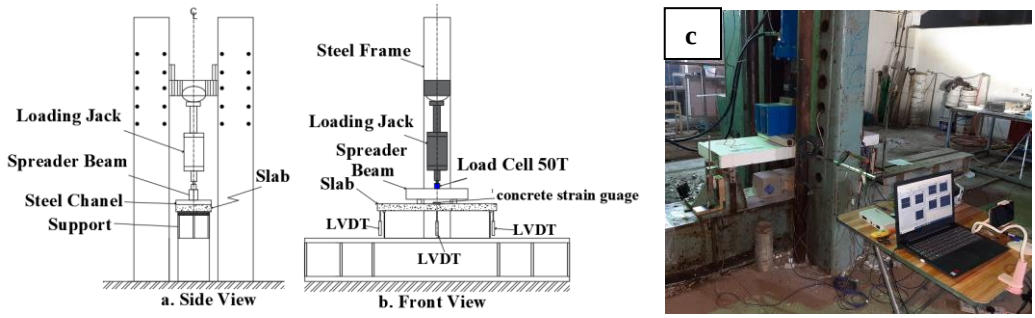

Figure 7. **(a, b)** Schematic test set up, **(c)** A slab before testing

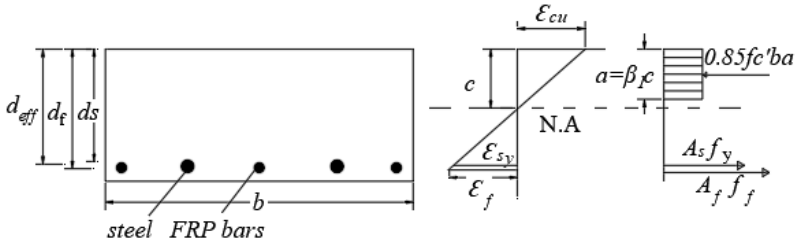

Figure 8. Strain-stress distribution model for combined steel-BFRP RC one-way slab

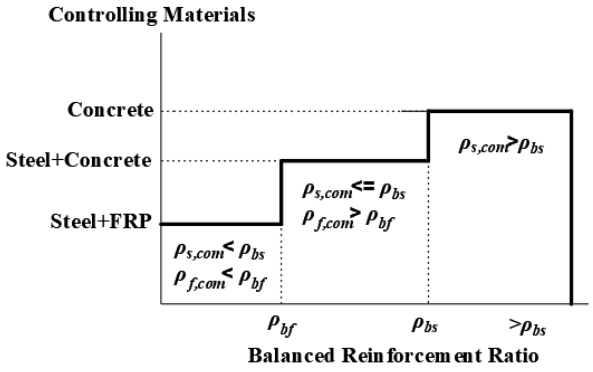

Figure 9. Theoretical analysis of failure modes

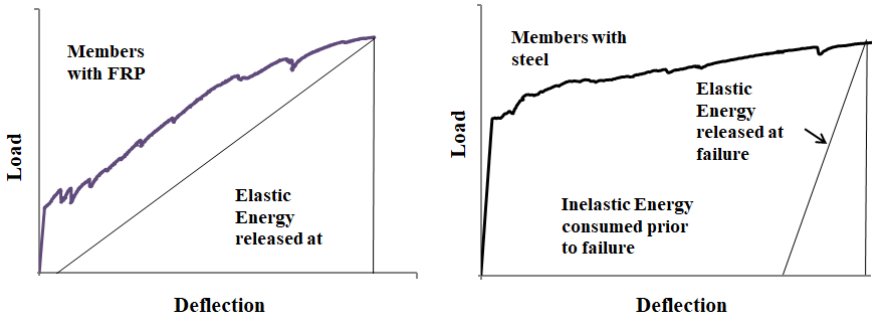

Figure 10. Energy released at failure in members with steel or FRP bars

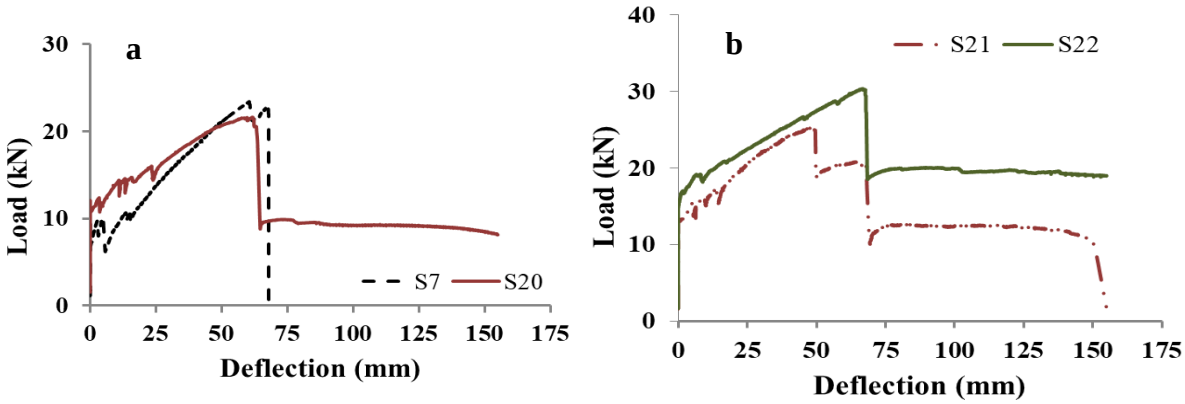

Figure 11. (a, b) Load-deflection curves of slabs in group A

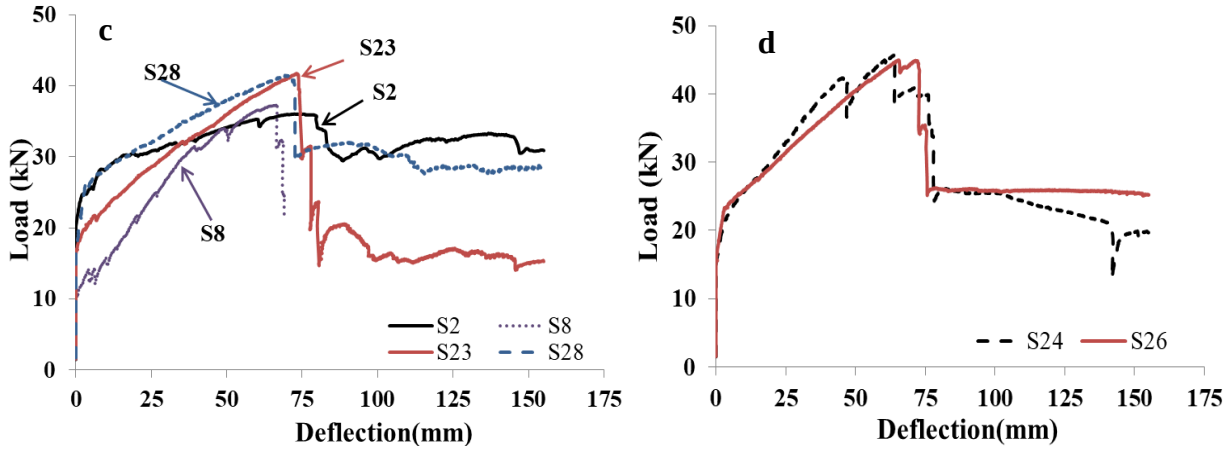

Figure 12. (c and d) Load-deflection curves of slabs in group B

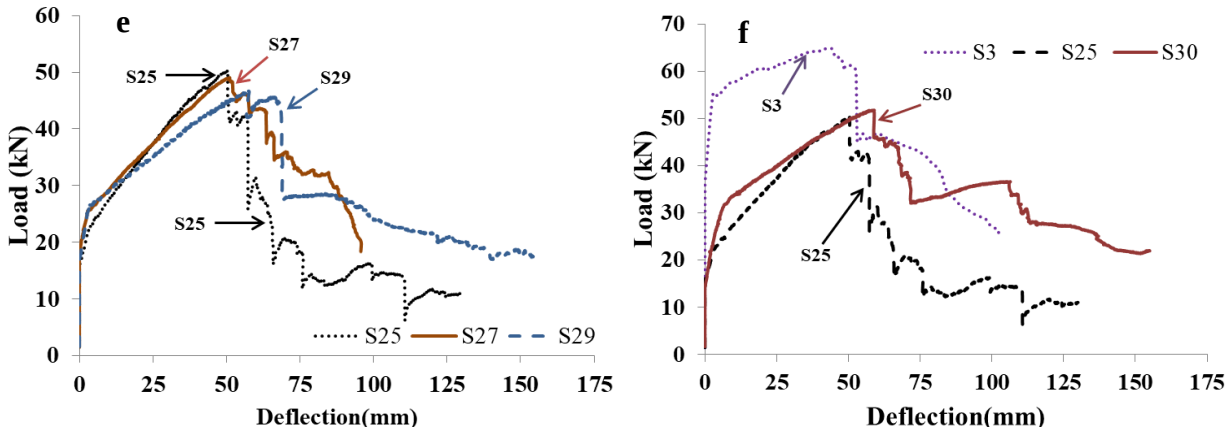

Figure 13. (e and f) Load-deflection curves of slabs in group C and D

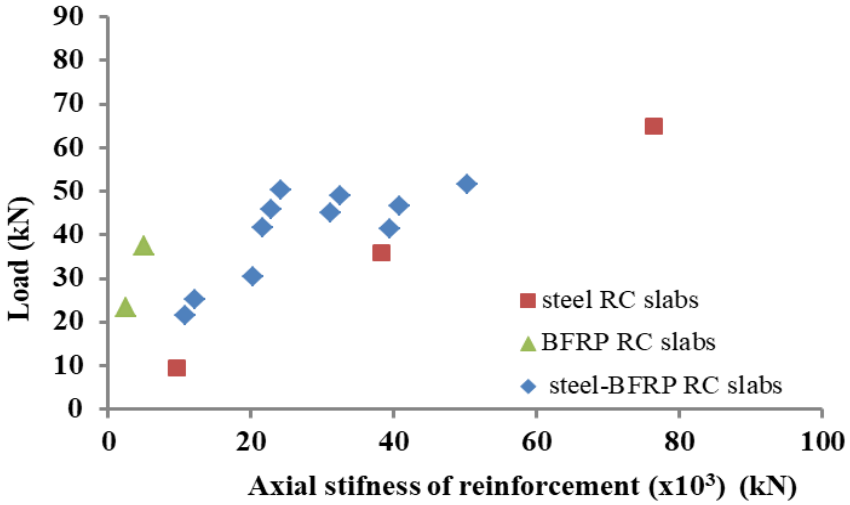

Figure 14. Load-axial stiffness of reinforcement of all the slabs

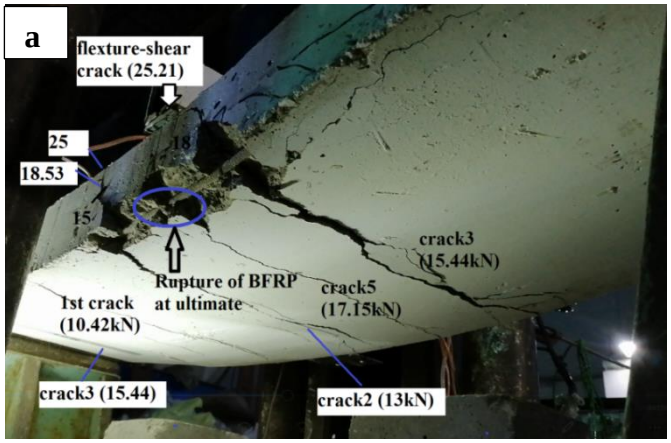
a
flexture-shear crack (25.21)
25
18.53
18
15
Rupture of BFRP at ultimate
crack3 (15.44kN)
crack5 (17.15kN)
1st crack (10.42kN)
crack3 (15.44)
crack2 (13kN)

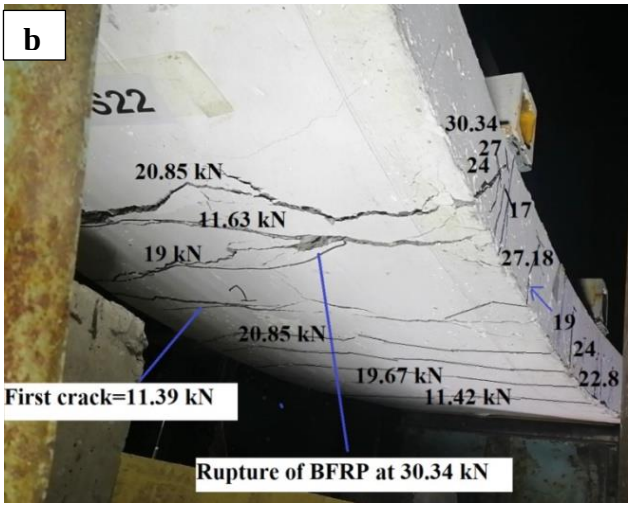
b
S22
30.34
27
24
20.85 kN
17
11.63 kN
19 kN
27.18
19
20.85 kN
24
19.67 kN
22.8
11.42 kN
First crack=11.39 kN
Rupture of BFRP at 30.34 kN

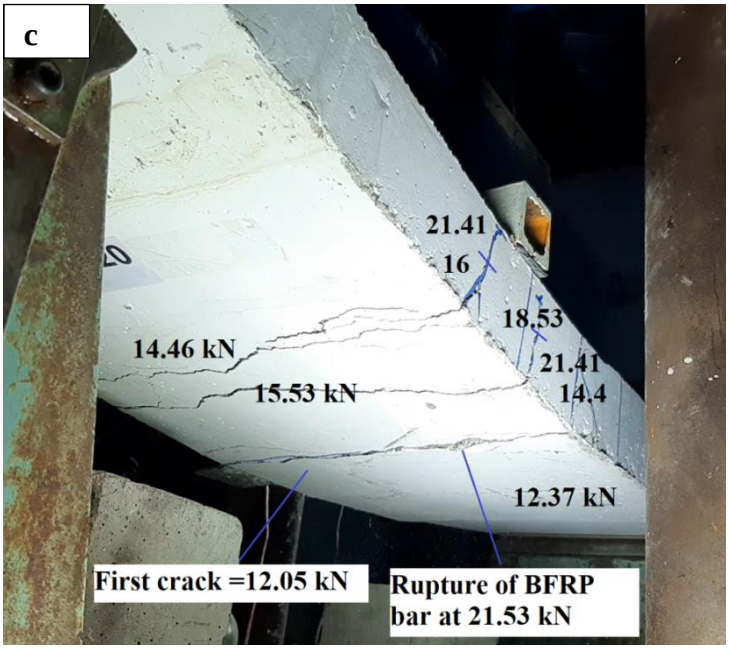
c
21.41
16
18.53
14.46 kN
21.41
15.53 kN
14.4
12.37 kN
First crack =12.05 kN
Rupture of BFRP bar at 21.53 kN

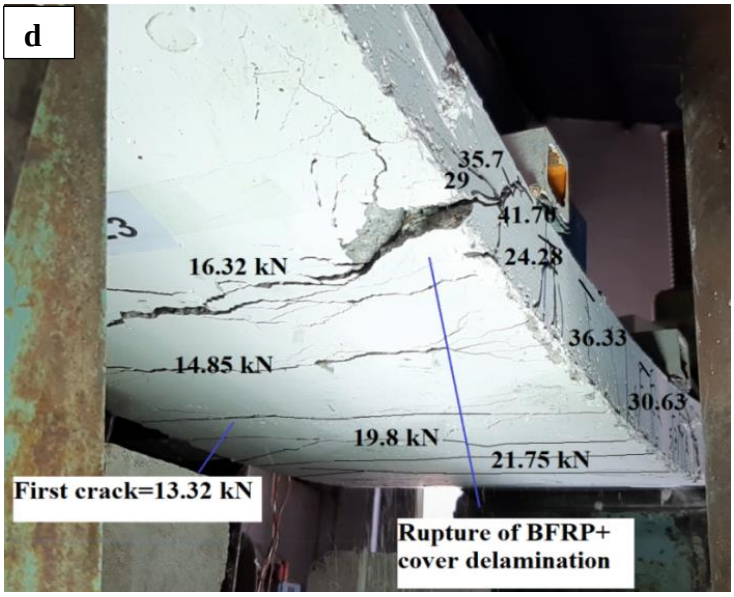
d
35.7
29
41.70
24.28
16.32 kN
36.33
14.85 kN
30.63
19.8 kN
21.75 kN
First crack=13.32 kN
Rupture of BFRP+
cover delamination

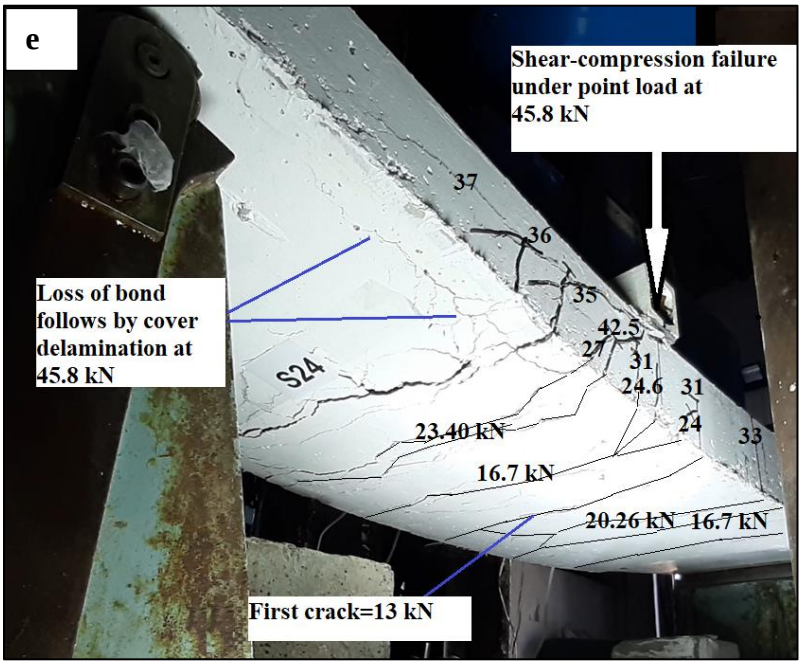
e
Shear-compression failure
under point load at
45.8 kN
37
36
35
42.5
27
31
24.6
31
24
33
Loss of bond
follows by cover
delamination at
45.8 kN
S24
23.40 kN
16.7 kN
20.26 kN
16.7 kN
First crack=13 kN

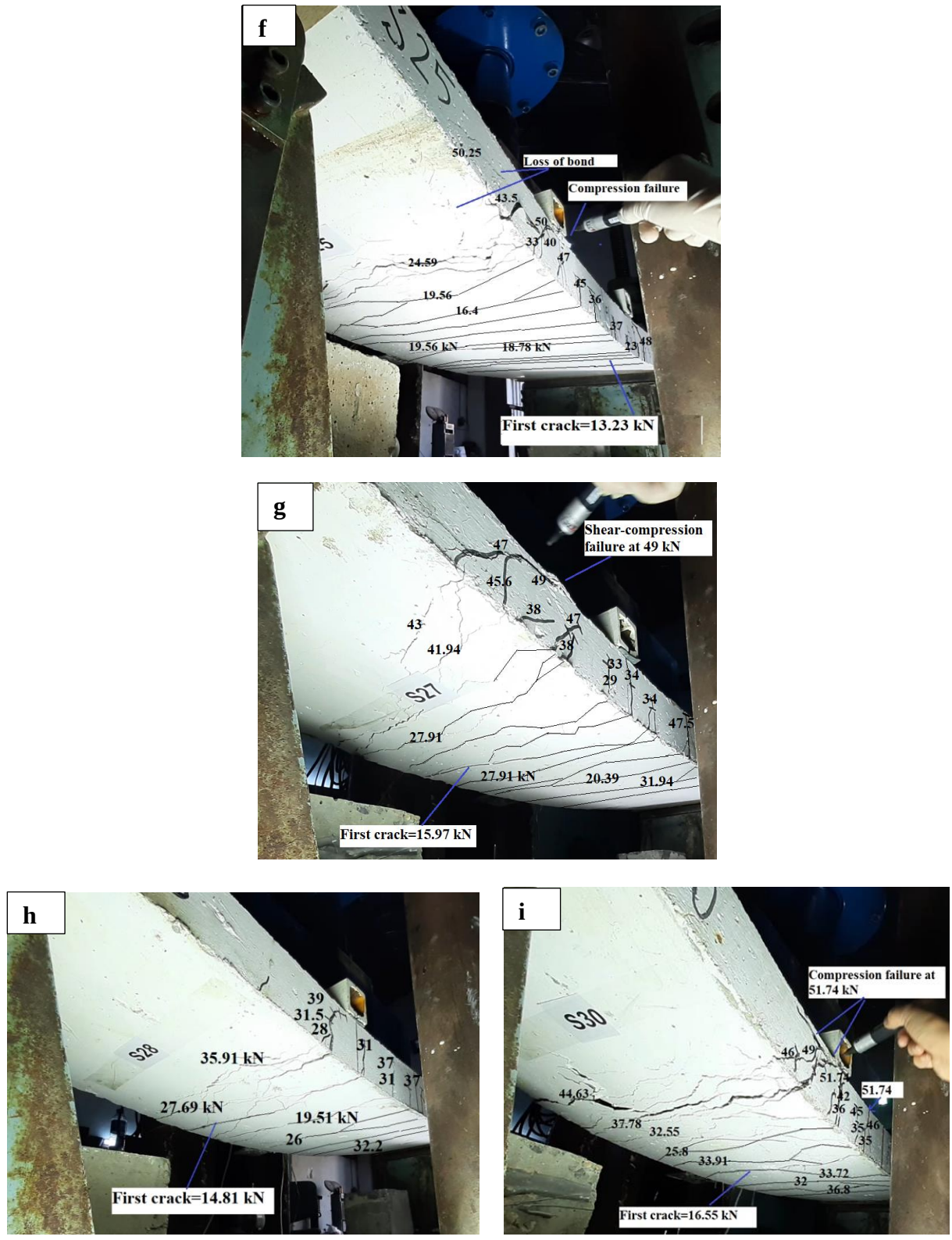

Figure 15. Failure modes of combined reinforced slabs with cracking loads and patterns **(a)** S21, **(b)** S22, **(c)** S20, **(d)** S23, **(e)** S24, **(f)** S25, **(g)** S27, **(h)** S28, **(i)** S30

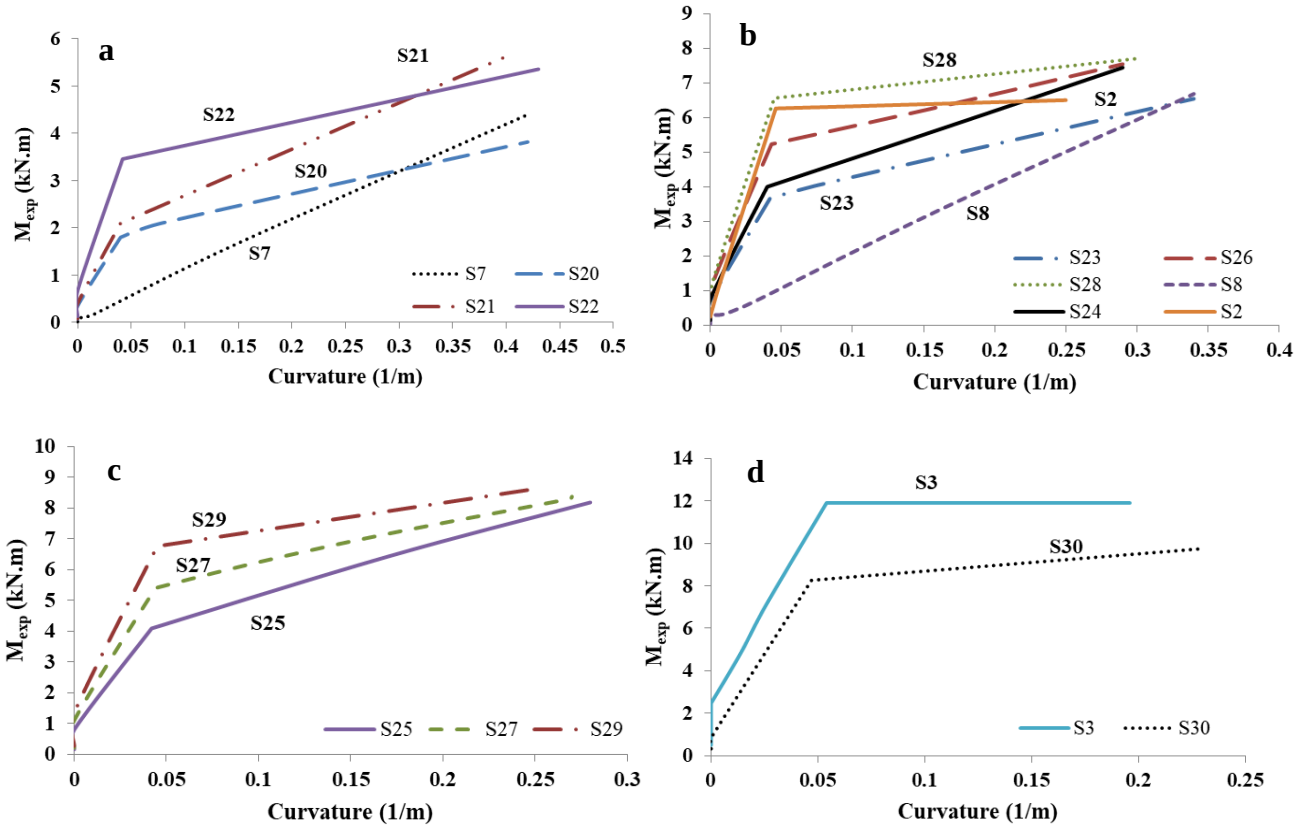

Figure 16. Moment-curvature relationships **(a)** group A, **(b)** group B, **(c)** group C, **(d)** group D

Table 1. Details of all the tested slabs

Slabs notation	Types of Reinf.	A_s (mm^2)	A_f (mm^2)	*fc'* (MPa) at testing day
S2-T0.724	Steel	191.2		46.00
S3-T1.448	Steel	382.4		46.00
S7-B0.211	BFRP		56.5	50.72
S8-B0.422	BFRP		113	53.67
S20-T0.18/B0.105	steel+BFRP	47.8	28.3	53.47
S21-T0.18/B0.211	steel+BFRP	47.8	56.5	53.47
S22-T0.362/B0.105	steel+BFRP	95.6	28.3	53.67
S23-T0.362/B0.211	steel+BFRP	95.6	56.5	53.47
S24-T0.362/B0.316	steel+BFRP	95.6	84.8	53.47
S25-T0.362/B0.42	steel+BFRP	95.6	113	53.47
S26-T0.543/B0.211	steel+BFRP	143.4	56.5	53.47
S27-T0.543/B0.316	steel+BFRP	143.4	84.8	53.47
S28-T0.724/B0.105	steel+BFRP	191.2	28.3	53.47
S29-T0.724/B0.211	steel+BFRP	191.2	56.5	53.47
S30-T0.905/B0.211	steel+BFRP	239	56.5	53.47

Table 2. Concrete mix proportions

Ingredients	Cement	Fine agg.	Coarse agg.	Water	Density of concrete kg/m^3	Slump (mm)	f_{cu} MPa (28 days)	f_c' MPa (28 days)
kg/m^3	460	944	713	230	2375	130-140	40	37
Ratio	1	2.03	1.53	0.5				

Table 3. Properties of longitudinal reinforcement

Bar type	Diameter (mm)	Yield strength (MPa)	Ultimate tensile strength f_{fu} (MPa)	Ultimate strain (%)	Elastic modulus E_f (GPa)
BFRP	6		1200	2.6	45
Steel	7.8	522			200

Table 4. Experimental and theoretical loads with modes of failure for all the slabs

Slabs notation	A_s/A_f	P_{cr} *(KN)*	P_{th} *(KN)*	P_{exp} *(KN)*	P_{th}/P_{exp}	P_{cr}/P_{exp}	*Modes of Failure*
S2-T0.724		16.38	31.34	36.01	0.87	0.45	*Steel yielding+ Concrete crushing
S3-T1.448		23.08	59.48	64.87	0.92	0.36	*Steel yielding +Concrete crushing
S7-B0.211		9.97	24.04	23.47	1.02	0.42	*BFRP rupture+ Concrete crushing
S8-B0.422		12.11	33.40	37.37	0.89	0.32	**Shear-Compression failure
S20-T0.18/B0.105	1.69	12.05	19.07	21.53	0.89	0.56	*Steel yielding+ BFRP rupture+ Concrete crushing
S21-T0.18/B0.211	0.85	12.37	28.08	25.26	1.11	0.49	*Steel yielding + BFRP rupture +Cover delamination+ shear failure
S22-T0.362/B0.105	3.38	10.68	26.81	30.34	0.88	0.35	*Steel yielding + BFRP rupture+ Concrete crushing
S23-T0.362/B0.211	1.69	13.32	32.69	41.74	0.78	0.32	*Steel yielding +Concrete crushing+ BFRP rupture
S24-T0.362/B0.316	1.13	11.16	37.17	45.79	0.81	0.24	**Steel yielding + (shear-compression failure)
S25-T0.362/B0.42	0.85	13.23	40.86	50.25	0.81	0.26	*Steel yielding+ Concrete crushing (Compression failure under point load)
S26-T0.543/B0.211	2.54	13.12	37.77	45	0.84	0.29	*Steel yielding + Concrete crushing
S27-T0.543/B0.316	1.69	15.97	41.91	49	0.85	0.33	**Steel yielding+ Shear-compression failure
S28-T0.724/B0.105	6.77	14.81	38.55	41.47	0.93	0.36	*Steel yielding + Concrete crushing
S29-T0.724/B0.211	3.38	16.22	43.21	46.68	0.93	0.35	*Steel yielding+ Concrete crushing (compression failure under point load)
S30-T0.905/B0.211	4.23	16.55	48.93	51.74	0.95	0.32	**Steel yielding + Compression failure

*Primarily failed in flexure

**Primarily failed in flexure and secondarily in shear

Table 5. Classification of the slabs in groups based on calculated theoretical reinforcement ratios

Groups	Slabs	$\rho_{f,com}$ (%)	ρ_{bf} (%)	ρ_{eff} (%)	ρ_{bs} (%)	Aim of Investigation
A	S7-B0.211	0.21	0.25	-	-	Load-deflection behavior and ductility improvement in slabs with under and balanced reinforcement ratio with $\rho_{f,com} \leq \rho_{bf}$
	S20-T0.18/B0.105	0.18	0.26	0.42	3.10	
	S21-T0.18/B0.211	0.29	0.26	0.67	3.10	
	S22-T0.362/B0.105	0.26	0.26	0.60	3.10	
B	S2-T0.724	-	-	0.73	2.89	Effects of over reinforcement ratio ($\rho_{f,com}$>1.4ρ_{bf}) and ratio of A_s/A_f on load-deflection behavior and ductility improvement
	S8-B0.422	0.42	0.26	-	-	
	S24-T0.362/B0.316	0.47	0.26	1.09	3.10	
	S23-T0.362/B0.211	0.37	0.26	0.85	3.10	
	S26-T0.543/B0.211	0.44	0.26	1.03	3.10	
	S28-T0.724/B0.105	0.42	0.26	0.96	3.10	
C	S25-T0.362/B0.42	0.58	0.26	1.34	3.10	Effects of higher degree of over-reinforcement with ($\rho_{f,com} > 2\ \rho_{bf}$) and ratio of A_s/A_f on load-deflection behavior and ductility
	S27-T0.543/B0.316	0.55	0.26	1.27	3.10	
	S29-T0.724/B0.211	0.52	0.26	1.21	3.10	
D	S3-T1.448		-	1.45	3.10	Effect of higher degree of over-reinforcement with ($\rho_{f,com} > 2\ \rho_{bf}$) on load-deflection behavior
	S30-T0.905/B0.211	0.6	0.26	1.40	3.10	

Table 6. Ductility measurements for all the groups

Groups	Slabs	A_s/A_f	Δ_y (mm)	Δ_u (mm)	(μ)	Δ_u/L	$D.F_{exp}$	$D.F_{th}$
A	S7-B0.211	-	-	60.40	-	50.3E-3	19.12	24.00
	S20-T0.18/B0.105	1.69	6.8	61.7	9.03	51.4E-3	5.20	5.89
	S21-T0.18/B0.211	0.85	-	48.00	-	40.0E-3	6.92	8.47
	S22-T0.362/B0.105	3.38	12.6	66.76	5.30	55.6E-3	5.00	7.00
B	S2-T0.724	-	5.8	72.8	12.56	60.7E-3	-	-
	S8-B0.422	-	6.9	66.8	-	55.7E-3	10.00	10.72
	S24-T0.362/B0.316	1.13	6.9	64.1	9.25	53.4E-3	8.00	8.80
	S23-T0.362/B0.211	1.69	4.0	73.1	18.27	60.9E-3	5.24	7.27
	S26-T0.543/B0.211	2.54	3.1	65.5	20.85	54.6E-3	5.20	7.00
	S28-T0.724/B0.105	6.76	3.0	69.3	22.80	57.7E-3	5.03	6.45
C	S25-T0.362/B0.42	0.85	3.1	50.5	16.28	42.1E-3	7.11	7.80
	S27-T0.543/B0.316	1.69	3.2	51.1	15.83	42.6E-3	8.26	10.00
	S29-T0.724/B0.211	3.38	3.5	57.5	16.33	47.9E-3	8.34	11.13
D	S3-T1.448		3.3	43.6	13.17	36.3E-3		
	S30-T0.905/B0.211	4.23	5.2	58.5	11.2	48.7E-3	8.60	13.00